Foxa2 lineage$^+$ mesendoderm forms a competitive pulmonary mesenchyme niche crucial for generating the entire lungs

Akihiro Miura[1, 2], Hemanta Sarmah[1], Junichi Tanaka[1], Youngmin Hwang[1], Anri Sawada, [1] Yuko Shimamura[1], Yinshan Fang[1], Dai Shimizu[2], Zurab Ninish[1], Jake Le Suer[3, 4], Nicole C. Dubois[5], Jennifer Davis[6], Shinichi Toyooka[2], Jun Wu[7], Jianwen Que[1], Finn J. Hawkins[3, 4], Chyuan-Sheng Lin[8], Munemasa Mori[1] †

1 Columbia Center for Human Development and Division of Pulmonary, Allergy, Critical Care, Department of Medicine, Columbia University Medical Center, New York, NY 10032, USA.
2 Department of Thoracic, Breast and Endocrinological Surgery, Okayama University Graduate School of Medicine, Dentistry and Pharmaceutical Sciences, Okayama, 7008558, Japan.
3 The Pulmonary Center and Department of Medicine, Boston University School of Medicine, Boston, MA 02118, USA
4 Center for Regenerative Medicine, Boston University and Boston Medical Center, Boston, MA 02118, USA
5 Department of Cell, Developmental and Regenerative Biology, Icahn School of Medicine at Mount Sinai, New York, NY 10029, USA.
6 Department of Pathology, University of Washington, Seattle, WA 98109, USA.
7 Department of Molecular Biology, University of Texas Southwestern Medical Center, Dallas, TX, USA
8 Bernard and Shirlee Brown Glaucoma Laboratory, Department of Pathology and Cell Biology, College of Physicians and Surgeons, Columbia University Irving Medical Center, New York, NY 10032, USA.

† To whom correspondence should be addressed:
Munemasa Mori, M.D., Ph.D.
650W 168th St, New York, NY 10032, USA
E-mail: mm4452@cumc.columbia.edu

Summary

Millions worldwide suffer from incurable lung diseases, and organ transplantation remains their only hope. However, there has been an absolute shortage of donor lungs and unmet needs for transplantable lung generation composed of tissue-specific mesenchyme, epithelium, and endothelium. Elucidation of lung precursor traits during development can lead to solving this issue. Using lineage-tracing mice, we discovered that gastrulating Foxa2 lineage$^+$ Pdgfrα$^+$ mesendoderm forms the competitive mesenchymal lung niche. We further evidenced that Foxa2$^+$Pdgfrα$^+$ mesendoderm is an evolutionarily-conserved niche during human iPSC-derived lung differentiation. The Fgfr2 gene depletion, specifically in the Foxa2 lineage, showed lung agenesis phenotype. Strikingly, donor iPSCs injection into those blastocysts complemented endodermal and mesodermal defective lung organ niches that efficiently led to the entire lung generation. Together, targeting Foxa2 lineage for lung generation is a novel paradigm, holding a grand promise for future human whole lung generation in large animals using human iPSCs.

KEYWORDS (3-10)
Entire lung generation
Conditional blastocyst complementation
Lung mesenchyme precursors
Mesendoderm

INTRODUCTION

Tissue regeneration to treat various intractable diseases has long been challenging[1–5]. Organ bioengineering strategy based on recellularizing tissue-specific progenitors into the decellularized scaffolds, induced pluripotent stem cell (iPSC)-derived organoids, or 3d-bioprinters are the next-generation tissue transplant therapies[3,6–8]. Even with these techniques, however, the mammalian lung is one of the most difficult organs to replicate because of its anatomical complexity and cellular diversity. It contains hundreds of airway branches and a thin micron-sized alveolar layer of inflated and well-vascularized alveoli composed of billions of cells from more than 50 different cell types[6,9–11]. Despite the worldwide donor organ shortage for lung transplantation, no technology has produced whole lungs composed of tissue-specific mesenchymal, epithelial, and endothelial systems.

Blastocyst complementation (BC) has been proposed as a promising option for tissue-specific niche completion[12]. This unique technology has been further developed into intra- and interspecies organ generations such as kidney, pancreas, and blood vessels[13–16]. However, the production of entire organs, including tissue-specific epithelium, endothelium, and mesenchyme, was still difficult. Unfortunately, even with blastocyst complementation, the lungs produced were non-functional and very inefficient, and in addition, the chimeric lungs contained a significant amount of host-derived tissue[17,18]. Previously, we established a sophisticated BC technique, the conditional blastocyst complementation (CBC) approach, that targets specific lineages complemented by donor pluripotent stem cells[19]. Using lineage-specific drivers of lung endoderm in CBCs avoids the effects of genetic manipulation in non-target organs for the generation of empty organ niches that lead to functional chimeric lung generation.[20,21]. However, most of the lung mesenchyme and endothelium were still derived mainly from the host cells, which was the severe limitation of CBC[19]. Given that the CBC approach targeted endodermal lungs, we speculated that this limitation was due to a significant gap in our knowledge of the origin of all lung cell types, especially pulmonary mesenchyme, including endothelium, a critical tissue component that causes hyperacute rejection of lung transplants. To overcome this critical issue, we explored whole lineage traits of the lung parenchyma and mesenchyme, the major components of the lung, that could lead to whole-lung production.

We hypothesized the existence of a single bona fide lung precursor cell lineage (BFL) that permits all cell type differentiation in the vacant lung organ niche leading to the generation of whole lungs.

During development, lung epithelial and mesenchymal precursors interact to initiate an elaborate developmental program of organogenesis that includes differentiation, pattern formation, progenitor cell expansion, and differentiation. The lung epithelial origin is derived from the definitive endoderm (DE), the entire epithelial precursor of the gut, classically labeled by Forkhead Box A2 (Foxa2)[22,23]. Multiple genetic studies using Sonic Hedgehog (Shh) Cre lineage-tracing mice have also shown that the entire Nkx2-1+ lung and tracheal epithelial primordium arises from Shh^{+} DE.

The lung mesenchyme primordium is derived from $Wnt2^{+}$ $Isl1^{+}$ cardiopulmonary progenitors (CPP). CPP is the derivative of $Osr1^{+}$ $Nkx6\text{-}1^{+}Barx1^{-}$ $Wnt4^{low}$ foregut lung mesoderm that arises from lateral plate mesoderm (LPM)[24]. While DE and LPM arise from primitive streaks (PS) during gastrulation, the exact lineage origin of LPM has been a complete mystery.

Mesendoderm is a bipotent transitional state between the PS and nascent mesoderm labeled by Mixl1, Pdgfrα, and Brachyury (T) during gastrulation that can give rise to both DE and mesoderm[25,26]. Pdgfrα is expressed in the epiblast-derived mesendoderm, the primitive endoderm

(PrE), and its extra-embryonic endoderm derivatives, such as parietal and visceral endoderm, around E5.5~E7.5. Foxa2 plays a pivotal role in alveolarization and airway goblet cell expansion[27], while there was a significant knowledge gap regarding Foxa2 lineage during lung development.

RESULTS

Pdgfrα$^+$ lineage during gastrulation gives rise to the entire lung mesenchyme, and the Foxa2 lineage overlaps the Pdgfrα$^+$ mesendoderm niche.

To determine the origin of LPM and pulmonary endothelium for the whole lung generation via BFL, we performed lung mesenchyme precursor lineage-tracing analysis using *Pdgfrα$^{CreERT2/+}$; Rosa$^{tdTomato/+}$* mice. Surprisingly, tamoxifen injection at E5.5 labeled the entire lung mesenchyme with tdTomato at E14.5 (Figures 1A and 1B). This result suggested that the origin of the whole lung mesenchyme is the Pdgfrα lineage around early-to-mid-streak-stage embryos. tdTomato labeled the entire pulmonary mesenchyme, including Sma$^+$ airway smooth muscle cells, Pdgfrβ$^+$ pulmonary mesenchyme, and VE-cadherin$^+$ vascular endothelial cells (Figure 1B). In addition, the Pdgfrα lineage only partially labels the lung epithelium (Figure 1B, arrows), suggesting that the contribution of the Pdgfrα lineage to the lung endoderm is low. It suggests that Pdgfrα is difficult to define as a BFL because of its low contribution to the lung epithelium.

Single-cell RNA-seq (scRNA-seq) analysis using Foxa2-Venus fusion protein reporter mice indicated that the Foxa2 lineage might give rise to LPM and DE [28]. Given that Foxa2 and Pdgfrα are expressed during the conversion from mesendoderm to mesenchyme[25,28–30], we used Foxa2-lineage tracing mice (*Foxa2$^{Cre/+}$; Rosa$^{tdTomato/+}$*)[31] to determine whether the Foxa2-lineage would label Mixl1$^+$ or Pdgfrα$^+$ mesendoderm around E6.25~7.0 during gastrulation. Notably, Foxa2-lineage-driven tdTomato labels a part of the Pdgfrα$^+$ mesendoderm of the primitive streak (PS) around E6.25~E6.5 relatively early-streak-stage embryos (Figure 1C, arrow). In the E6.5~E7.0 mid-to-late-streak-stage PS region (Figure 1D, dotted lines), Foxa2-lineage-derived tdTomato were found in the PS and Pdgfrα$^+$ adjacent nascent mesoderm, suggesting that Foxa2 lineage-labeled Pdgfrα$^+$ cells ingresses from PS to nascent mesoderm regions (Figure 1D, arrowheads). These data are reminiscent of the definition of mesendoderm [25,26]. Our result indicates that the Foxa2 lineage-labeled Pdgfrα$^+$ cells are the mesendoderm, most likely the derivative of posterior epiblasts, since Foxa2 is expressed only in the posterior epiblasts before gastrulation [28]. Further Immunostaining analysis of the sequential sections of mid-streak-stage E6.5~6.75 embryos confirmed that the Foxa2 lineage appeared in the distal portion of Mixl1-weakly-positive mesendoderm (Figures 1E and 1F, arrows) at anterior primitive streak (APS) besides the Foxa2 protein-expressing DE (Figures 1E and 1F, arrowheads). Based on our Pdgfrα$^+$ lineage tracing data, we further examined whether Foxa2-lineage would label lung mesenchyme.

Foxa2-lineage labeling increased during lung development, leading to occupy the entire lung epithelium and half of the lung mesenchyme, including lung endothelium

Foxa2-lineage tracing mice (*Foxa2$^{Cre/+}$; Rosa$^{tdTomato/+}$*) faithfully target Nkx2-5$^+$ cardiac progenitors, associated with the origin of Wnt2$^+$ Isl1$^+$ CPP[32,33] lung mesenchyme. However, there was no conclusive evidence of whether Foxa2-lineage-derived mesendoderm can give rise to Wnt2$^+$ Isl1$^+$ CPP[32,33]. Using the Foxa2-lineage tracing mice, we found from immunostaining that Foxa2 lineage labeling occupies the entire lung epithelium and most of the lung mesenchyme at E16.5 (Figures 2A-C). Quantitative analyses by flow cytometry in the E14.5 developing lungs of Foxa2-lineage tracing mice showed that Foxa2-lineage labeled almost the entire lung epithelium

(89.6%± 1.80) and the partial lung mesenchyme (24.1%± 5.31), including endothelial cells (18.3 %± 8.05) (Figure 2D). Contrary to expectations, Foxa2-lineage labeled cells increased dramatically throughout lung development (Figure 2E). In adulthood, the Foxa2-lineage labeling reached about 98.98%± 0.171 in lung epithelium, 45.43%± 7.30 in lung mesenchyme, and 61.48%± 9.49 in lung vascular endothelial cells, with more than two-fold change in the lung endothelium compared with E14.5 (Figure 2E). Morphometric analysis of immunostaining further confirmed that Foxa2 lineage marked about 30% of E14.5 multiple cell types of lung mesenchyme: Sma^+ smooth muscle cells (24.9%± 8.50), VE-cadherin$^+$ (39.3%± 12.5) or Pecam1$^+$ (36.6%± 11.1) endothelial cells, and Pdgfrβ$^+$ pericytes of the pulmonary arteries and pulmonary veins (41.4%± 10.5) (Figures 1F and 1G). Interestingly, no clear Foxa2 protein level expression was observed in the mesenchyme of the embryonic lungs (Figure S1A), consistent with previously reported Foxa2 protein expression patterns[27]. However, the LungMAP deposited single-cell RNA-seq database analysis showed a sporadic Foxa2 transcriptional expression pattern in developing lung mesenchyme, particularly in proliferating endothelium, on E15.5 and E17.5 (Figure S1B). To confirm this observation, we sorted the cell fraction of CD45$^-$ CD31$^-$ EPCAM$^-$ tdTomato$^+$ and CD45$^-$ CD31$^-$ EPCAM$^-$ tdTomato$^-$ from developing lung mesenchyme at E18.5. We observed a slight increase in the relative expression of *Foxa2* in the tdTomato$^+$ fraction of embryonic lung mesenchyme, which most likely contributed to the labeling in the Foxa2-lineage tracing mice (Figure S1C). These results suggest pulmonary mesenchymal progenitor cells turned on Foxa2 expression slightly at the mRNA level rather than the protein level, which led to a gradual increase in Foxa2 lineage labeling. Furthermore, tdTomato$^+$ endothelial cells were found to have a slightly higher proliferative capacity than tdTomato$^-$ cells (Figure S1D). These results suggest that Foxa2$^+$ pulmonary mesenchymal lineage gradually outcompetes Foxa2$^-$ lung mesenchyme progenitors throughout lung development, winning cell competition by the increased proliferative capacity.

Co-development of endodermal and mesodermal lung progenitors derived from MXIL1$^+$ PDGFRα^+ FOXA2$^+$ mesendoderm in the directed differentiation protocol using hiPSC

To determine whether Foxa2 or Pdgfrα mesoderm is an evolutionarily well-conserved niche that can give rise to both pulmonary endoderm and mesoderm, we modified a previously reported protocol to establish a pulmonary endoderm-mesoderm co-developmentally directed differentiation protocol[23,34–37] (Figure 3A). With this optimized protocol, various hiPSC lines were found to efficiently induce a lung bud-like appearance, indicated by NKX2-1+, in lung epithelial cells[36,37]. We found that on day10, TBX4$^+$ lung mesenchyme emerged and surrounded the NKX2-1$^+$SOX9$^+$ lung epithelium (Figure 3B and 3C). The qPCR kinetics analyses across the time point further supported the appearance of lung mesenchyme, represented by peak LPM marker expression peaked on day6~8; *OSR1, FGF10, BMP4, PDGFRα*, and smooth muscle cell markers peaked on day8~10; *ACTA2* and *PDGFRβ*, and CPP markers peaked on day8~12; *ISL1, WNT2, FOXF1,* and *TBX4*, peaked on days 10~14 simultaneously with pulmonary epithelial markers, *NKX2-1* and *CPM* (Figure 3D).

In this differentiation protocol, NKX2-1$^+$ lung endoderm and WNT2+TBX4$^+$ lung mesoderm were derived from the anteroventral endoderm and mesoderm at day 15 after Activin-mediated definitive endoderm and LPM induction, respectively[23,35]. During primordial streak induction from day0 to day3, cell surface markers of PDGFRα and EPCAM and intracellular FOXA2 and MIXL1 kinetics were analyzed by flow cytometry every 12 hours (Figure 3E). Briefly, 12 hours after the Activin induction, more than 60% of the EPCAM$^+$PDGFRα$^-$ primitive streak first turned on MIXL1, the mesendoderm marker[25,26]. Subsequently, the epithelial-mesenchymal

transition occurred 24 hours later, as represented by the PDGFRα induction in EPCAM^{+}MIXL1^{+} mesendoderm. After 36 hours, more than 90% of MIXL1+EPCAM+ mesoderm cells expressed PDGFRα. At the same time, expression of FOXA2 appeared in some of those mesoderm cells (Figures 3E and 3F). Thereafter, PDGFRα expression decreased, and 72 hours later, mutual FOXA2 induction appeared when EPCAM^{+}FOXA2^{+} DE and EPCAM^{-}FOXA2^{-} LPM were presented (Figure 3G). The dynamics of MIXL1, PDGFRα, and FOXA2 were further revealed by qPCR analysis (Figure 3H). These results suggest that PDGFRα^{+} and FOXA2^{+} expressing cells are redundant but distinct phases of mesoderm and can give rise to both endoderm and mesoderm lung cells in an evolutionarily conserved manner (Figure S4A).

Foxa2-driven Fgfr2 conditional knockout showed a lung agenesis phenotype

The evolutionary-conserved Foxa2-lineage^{+} mesendoderm forms DE with the competitive lung mesenchymal niche, suggesting that it may function as a BFL to generate the entire lungs after donor cells are injected into the vacant niche in the Foxa2 lineage. To explore this possibility, CBC was performed using Foxa2-driven Fgfr2-conditional knockout mice (*Foxa2*$^{Cre/+}$*; Fgfr2*$^{flox/flox}$, hereafter, *Foxa2*$^{Cre/+}$*; Fgfr2*^{cnull}). Mitotic signaling via Fgfr2 is required for both lung epithelium and mesenchyme, and systemic knockout mice of Fgf10 or Fgfr2 exhibit a phenotype of lung agenesis[38–41]. Based on the results of Foxa2 lineage tracking and the need for Fgfr2 signaling, it was predicted that *Foxa2*$^{Cre/+}$*; Fgfr2*^{cnull} mice would be used to generate vacant niches in both lung epithelium and mesenchyme. Indeed, they exhibited a lung agenesis phenotype (Figures S2A-S2C). However, we did not observe agenesis phenotype in other major internal organs related to the Fgfr2 systemic knockout phenotype (Figure S2D) [38–41].

Generation of the entire lungs in *Foxa2*-driven *Fgfr2*-deficient mice via CBC

To examine whether donor cells complement the lung agenesis phenotype, we generated nGFP^{+}iPSCs from Rosa$^{nT\text{-}nG}$ mice (hereafter, nGFP^{+}iPSCs) via Sendai virus-mediated reprogramming[23]. nGFP^{+}iPSCs were injected into mouse blastocysts (Figure 4A), and chimerism was analyzed at E17.5. Strikingly, donor nGFP^{+}iPSCs generated whole lungs in *Foxa2*$^{Cre/+}$*; Fgfr2*^{cnull} mice, but general chimerism on the skin was diverse (Figure 4B and S3A). Importantly, almost the entire lung epithelial, mesenchymal, and endothelial cell population at E17.5 was composed exclusively of nGFP^{+}iPSCs (Figures 4C and S3B). In contrast, wild-type, Shh-driven heterozygous, or knockout mice showed about 50-70% chimerism in the mesenchymal and endothelial lineages of the lung, but never constantly reached 100% (Figure 4C and 4D). Interestingly, although tdTomato^{+} Fgfr2 knockout mesenchymal cells sometimes remained in early lung development at E14.5, the percentage of Ki67^{+} proliferating cells was significantly higher in GFP^{+} donor cells compared to tdTomato^{+} host cells (Figures 4E – 4G). These results suggest that because the host niche loses competitiveness due to Fgfr2 depletion, generating a genetically deficient niche in the host's highly competitive endogenous Foxa2 mesenchyme effectively allows donor iPSCs to repopulate in all host-derived mesenchyme niches.

DISCUSSION

We provide a novel conceptual and lineage framework for the whole lung generation applicable to large animals. Our results are based on the BFL concept to reveal a previously unknown lineage trait of lung progenitors that leads to efficient generation of the entire lungs via the CBC. We envision that it is also possible to generate other whole organs via CBC by finding a common precursor lineage that can give rise to all cell types of a target organ niche. While pulmonary epithelial cell precursors were well-known to be DE in this field, the origin of pulmonary mesenchymal lineage precursors was a complete mystery. Targeting the endodermal lung lineage driven by Shh was insufficient to generate whole lungs, and chimeras remained formed in the mesodermal lung component [42]. The Shh-lineage traces putative DE-derived epithelial lineage but little lung mesenchyme (Figure S3C). Conversely, Pdgfrα-lineage is the origin of the entire lung mesoderm, including endothelium (Figures 1A and 1B)[19]. The analysis of embryonic development by scRNA-seq supported this idea [43] (Figure S4B). Our lineage tracing analysis revealed that Foxa2-lineage^{+} lung mesenchyme harbors a relatively-competitive, proliferative capacity compared to Foxa2 lineage^{-} Pdgfrα lineage^{+}-derived mesenchymal cells. Foxa2-lineage^{+} lung mesenchyme is derived from Foxa2 lineage^{+} Pdgfrα^{+} mesendoderm that provides unique competitive developmental potential during lung development. Presumably, the differential origin of lung mesenchyme; Foxa2 lineage^{-} Pdgfrα lineage^{+}-derived lung mesenchyme vs. Foxa2 lineage^{+} Pdgfrα lineage^{+}-mesendoderm derived lung mesenchyme may play a distinct role during lung development. For example, Foxa2 lineage^{-} Pdgfrα lineage^{+}-derived lung mesenchyme might have a pivotal role in initiating lung mesenchyme specification, but further analysis is required to conclude it. Depleting Fgfr2 in the Foxa2 lineage results in the loss of competitive function of Foxa2 lineage^{+} lung mesenchyme, which leads to the loss of competitiveness in most lung mesenchyme. This led to donor iPSCs outcompeting efficiently with the developing host pulmonary mesenchymal niche and efficiently generating whole lung organs.

Together, the Foxa2 lineage^{+} served as a mighty, potent BFL lineage sufficient for generating the entire lungs composed of lung epithelium, mesenchyme, including endothelium. Our strategy is promising for the future human whole lung generation in mice and large animals via a BFL-based CBC approach for modeling various lung diseases and transplantation therapy, respectively.

Acknowledgments

We thank Zurab Ninish for his technical assistance. We sincerely appreciate the generous support from Dr. Hiromitsu Nakauchi at Stanford University and the considerate support and scientific input from Dr. Wellington Cardoso at the Columbia Center for Human Development (CCHD) and the members of Cardoso's lab and CCHD. We acknowledge the support from the CCHD Medicine Microscopy core (MMC), Columbia Stem Cell Initiative (CSCI) Flow Cytometry core (SONY MA900), and Genetically Modified Mouse Model Shared Resource (GMMMSR) for blastocyst injection. This work was funded by NIH-NHLBI 1R01 HL148223-01, DoD PR190557, PR191133 to M. M., JSPS202080340, and The Uehara Memorial Foundation to A. M.

Author contributions

A.M. and M.M. designed all experiments; Z.N. and A.M. maintained mutant mice for the injection; C.S.L. performed blastocyst injection and embryo transfer; J.T., A.S., Y.S., Y.H., H.S., supported lineage-tracing, chimera analyses, and genotyping; H.S., D.S., and S. T. helped to generate mouse

and human iPSCs, J.S. and F.H. kept human iPSC-directed differentiation, N.D. provided Foxa2$^{Cre/+}$ mice, A.M. and M.M. wrote the paper; Y.H., H.S., J.W., J.Q., and F.H. gave crucial insights on the experiments and the manuscripts. There is no competing financial interest.

Declaration of interests

The authors declare no competing interests.

FIGURES

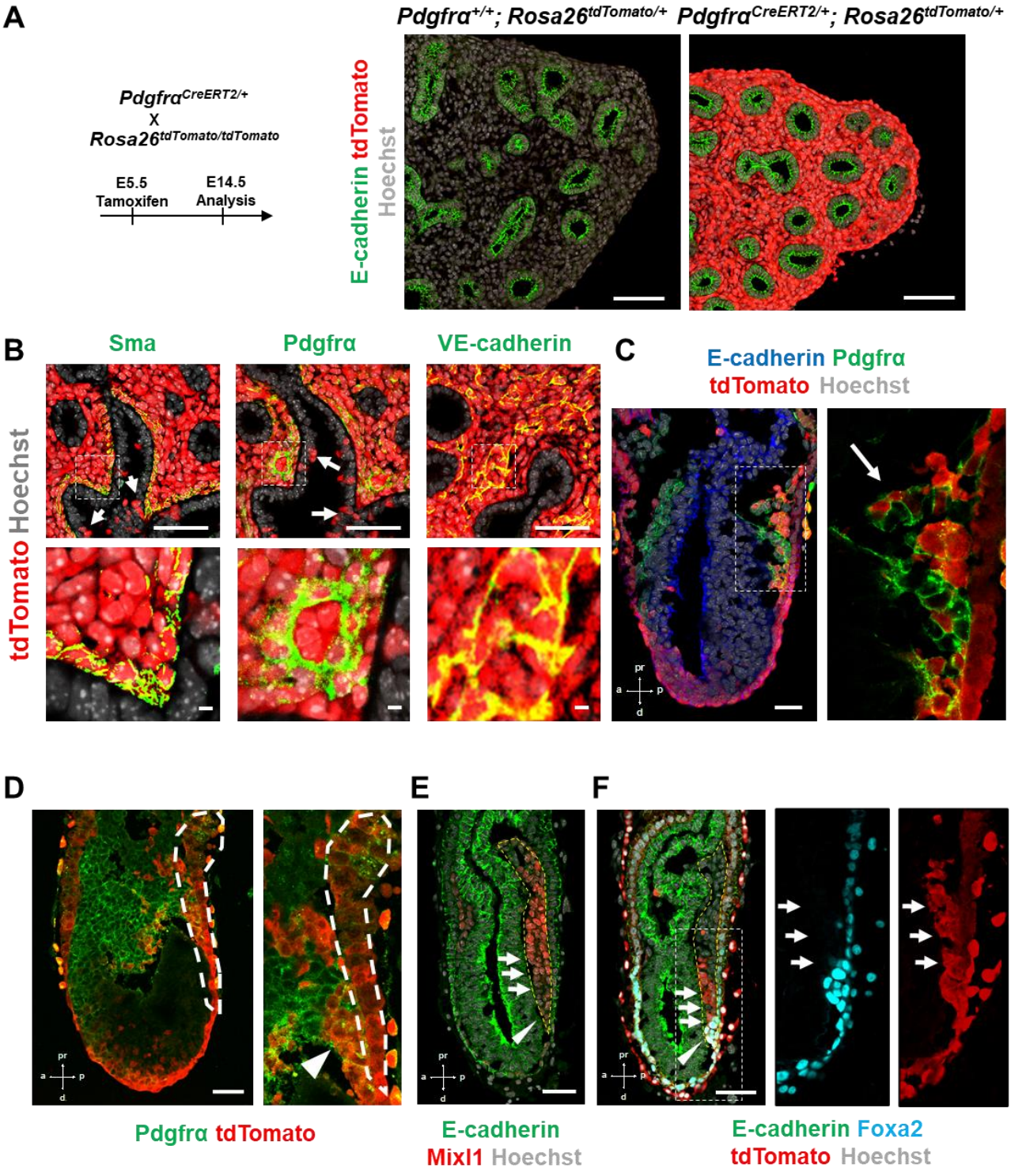

Figure 1. Pdgfrα lineage during gastrulation is the origin of the entire pulmonary mesenchyme, and Foxa2-lineage overlaps the Pdgfrα^{+} mesendoderm. (A) Left: Schematic of Tamoxifen administration (A-B). Representative Immunofluorescence (IF)-confocal imaging of E14.5 *Pdgfrα$^{CreERT2/+}$; Rosa26$^{tdTomato/+}$* lineage tracing mouse lungs (A, B). Tamoxifen administration at E5.5 labels Pdgfrα-lineage-driven tdTomato (red) in the entire lung mesenchyme (A), including Sma^{+} airway smooth muscle cells, Pdgfrα^{+} mesenchyme, and VE-cadherin^{+} capillaries (B). Pdgfrα-lineage also labeled a low proportion of epithelial cells (B, white arrows). Enlarged box: dotted box. Cre^{-} littermate control (A, middle panel) (*n = 3* per group). Scale bars: A, B = 100, 500μm. (C-F) Representative IF-confocal imaging of E6.25 (C), E7.0 (D), and E6.5 (E, F) from *Foxa2$^{Cre/+}$; Rosa26$^{tdTomato/+}$* mice. E-cadherin indicates epiblasts (C-F): (C) Foxa2-lineage (red) labeled Pdgfrα (green) expressing mesendoderm (arrow). (D) Foxa2-lineage labeled Pdgfrα^{+} cells and ingresses from primitive streak (PS) (dotted lines) to nascent mesoderm regions (arrowhead). (E) Mixl1 (red) expression in PS (yellow dotted area). (F) Sequential section of E: Enlarged box: Foxa2-lineage (red) marked the distal portion of the arteriolarizing PS that is a part of the MIxl1^{dim+} mesendoderm (E-F, arrowheads). (*n = 3* per group). Scale bars = 50μm.

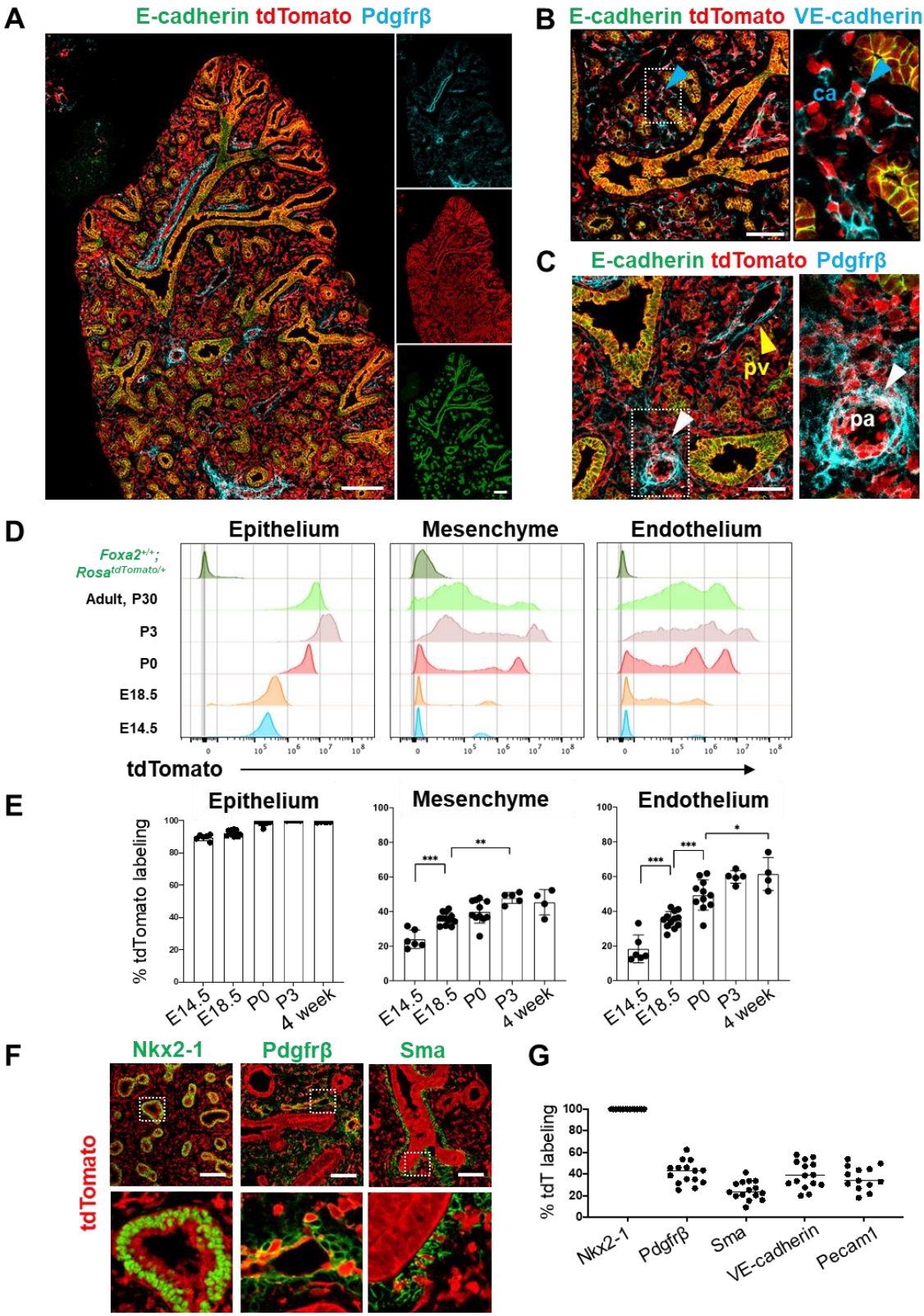

Figure 2. Foxa2-lineage gradually increased during lung development and labeled the entire lung epithelium and half of the mesenchyme. (A-C) IF-confocal imaging of E16.5 *Foxa2*$^{Cre/+}$*; Rosa*$^{tdTomato/+}$ embryonic lung: (A) Foxa2-lineage (red) labeled E-cadherin^{+} lung epithelium (green) entirely and Pfgfrβ^{+} mesenchyme (cyan) partially. (B) Foxa2-lineage partially labeled VE-cadherin^{+} capillary (ca) (enlarged box, blue arrowhead). (C) Foxa2-lineage labeled Pdgfrβ^{+} smooth muscle cells of the pulmonary artery (pa) (enlarged box, white arrowhead) and pulmonary vein (pv, yellow arrowhead). Scale bars (A), (B), and (C) = 200μm, 100μm, and 100μm, respectively. (D and E) Representative histograms and the graphs of FCM quantitative analyses for CD31^{-}Epcam^{+} lung epithelium, CD31^{-}Epcam^{-} mesenchyme, and CD31^{+}Epcam^{-} endothelium at E14.5, E18.5, P0, P3, and four weeks adult (n = 6, 12, 7, 5 and 4, independent biological replicates, respectively) of *Foxa2*$^{Cre/+}$*; Rosa*$^{tdTomato/+}$ mouse lungs. The gradual increase of % tdTomato^{+} lineage labeling in both lung mesenchyme and endothelium. Statistical analysis: one-way ANOVA with the Tukey post hoc test.; statistically significant if $*P < 0.05$, $**P < 0.01$ $***P < 0.001$, ns: non-significant. (F-G) IF-confocal imaging of E14.5 *Foxa2*$^{Cre/+}$*; Rosa*$^{tdTomato/+}$ embryonic lungs. tdTomato labeled entirely with lung epithelial markers Nkx2-1(left) but a relatively low proportion of mesenchyme (Pdgfrβ: middle, and Sma: right). (n = 3 per group). Scale bars = 50μm. Graphs in (G): The morphometric analysis: % of Foxa2-lineage labeling in Nkx2-1^{+}epithelial, Pdgfrβ^{+}mesenchyme, Sma^{+}airway smooth muscle, VE-Cadherin^{+} capillaries, or PECAM1^{+} arteries from E14.5 *Foxa2*$^{Cre/+}$*; Rosa*$^{tdTomato/+}$ lungs. (n = 3 per biological replicates, 5 fields per group).

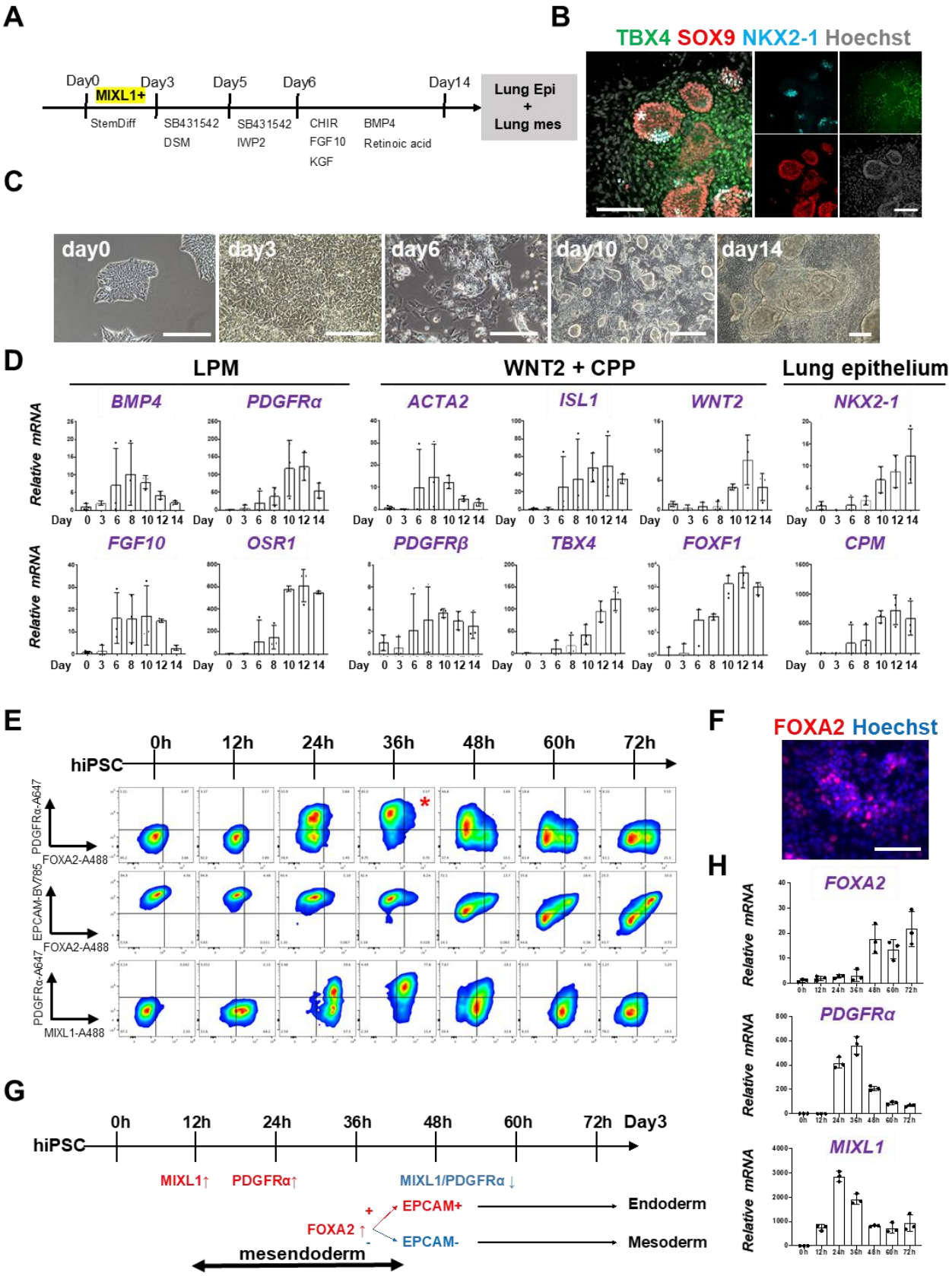

Figure 3. Co-development of endodermal and mesodermal lung progenitors derived from MXIL1$^+$ PDGFRα^+ FOXA2$^+$ mesendoderm in the directed differentiation protocol using hiPSC. (A) Schematic culture protocol of hiPSC-derived endodermal and mesodermal lung progenitor cell co-differentiation. (B) Representative IF-confocal imaging of differentiating hiPSCs at day 10 culture. Lung epithelium (NKX2-1), distal lung bud epithelium (SOX9), mesenchyme (TBX4), and nucleus (Hoechst) markers. The budding structures expressed SOX9 and partially NKX2-1 (asterisk), and monolayer cells expressed TBX4. (C) Representative phase-contrast images of the directed differentiation time course (D) qRT-PCR analyses of lung mesenchyme and epithelium markers in time course according to the protocol shown in (A). (E) FCM-based protein kinetic analyses during DE and LPM induction; MIXL1 expression preceded compared to PDGFRα or FOXA2. FOXA2 appearance in the subset of the PDGFRα$^+$ population (red asterisk). (*n = 3* independent experiments) (F) Representative IF imaging of 36 hours-cultured hiPSCs. (G) Schematic summary of flow cytometry analysis. (H) qRT-PCR analyses further confirmed the preceded *MIXL1* induction and subsequent expression of *PDGFRα* and *FOXA2*. All graphs: Data normalized by undifferentiated iPSCs. Each plot showed a different biological experiment. Error bars represent mean ±SD.

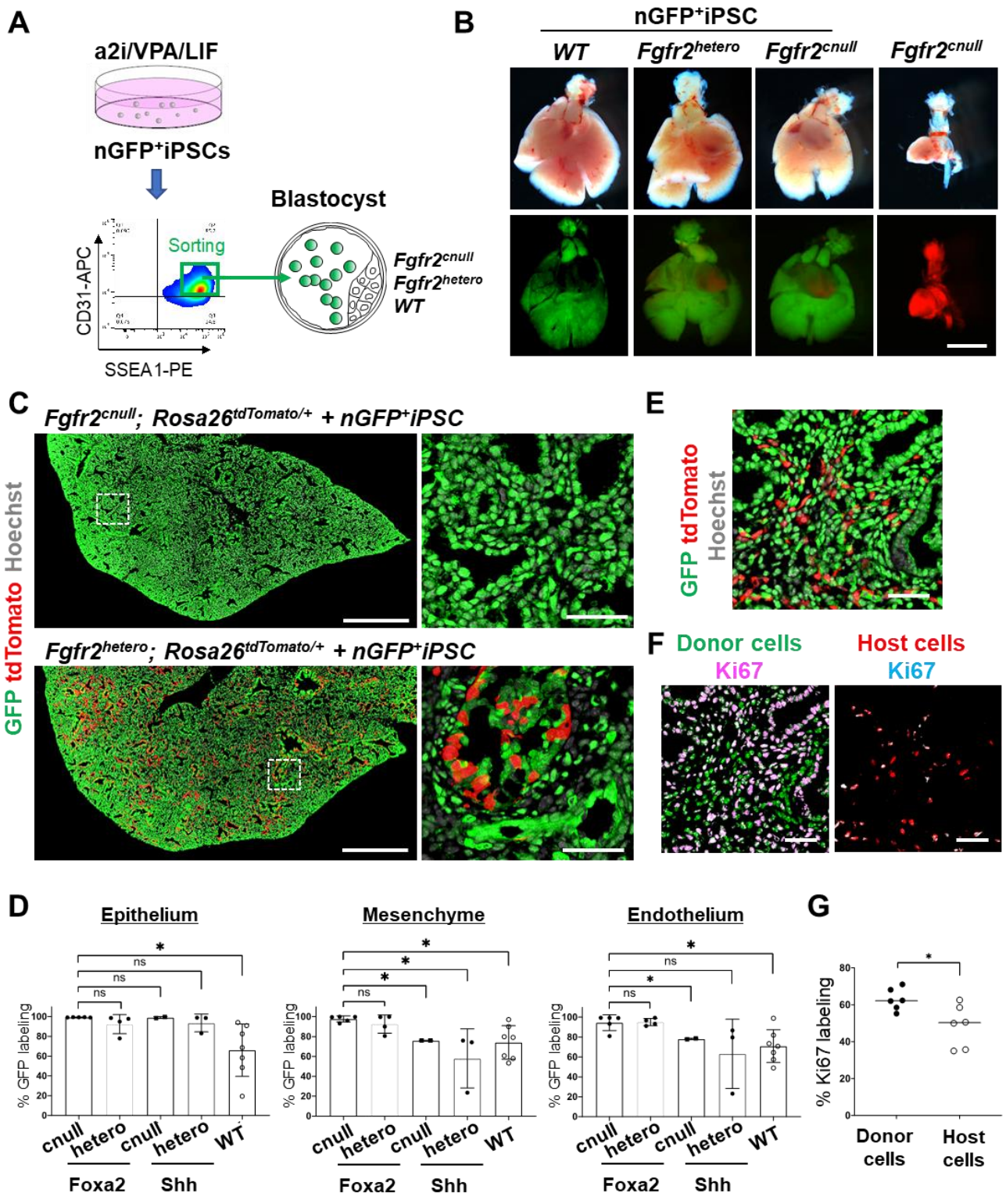

Figure 4. Generation of the entire lungs in *Foxa2*-driven *Fgfr2*-deficient mice via CBC.
(A) Schema of CBC experiment: a2i/VPA/LIF-treated SSEA1^{high} CD31^{high} nGFP^{+}iPSCs were sorted and injected into WT, *Fgfr2*^{hetero} (heterozygous: *Foxa2*$^{cre/+}$; *Fgfr2*$^{flox/+}$; *Rosa26*$^{tdTomato/+}$), and

Fgfr2^{cnull} (homozygous: *Foxa2*$^{cre/+}$; *Fgfr2*$^{flox/flox}$; *Rosa26*$^{tdTomato/+}$) blastocysts. (B) Gross morphology, GFP (green: donor nGFP^{+}iPSCs-derived signals), and tdTomato (host Foxa2-lineage-derived signals) fluorescence of freshly isolated lungs from E17.5 chimeric *WT*(left), *Fgfr2*^{hetero} (left middle), and *Fgfr2*^{cnull} (right middle) that were injected with nGFP^{+}iPSCs. Control: littermate *Fgfr2*^{cnull} mouse without nGFP^{+}iPSCs injection (right). (C) IF-confocal imaging of E17.5 *Fgfr2*^{cnull} or *Fgfr2*^{hetero} lungs injected with nGFP^{+}iPSCs. Dotted lines: enlarged images: Compared with littermate control holding host-derived cells (red), E17.5 *Fgfr2*^{cnull} lungs were entirely composed of donor-derived nGFP^{+} cells (green). (D) Graphs: % GFP in CD31^{-}Epcam^{+} lung epithelium, CD31^{-}Epcam^{-} mesenchyme, and CD31^{+}Epcam^{-} endothelium analyzed by flow cytometry. Each plot: a different biological animal. Statistical analyses: unpaired Student's t-test, significance at $*P < 0.05$, ns: non-significant. Nearly 100% of chimerism among the lung epithelium, endothelium, and mesenchyme only in *Foxa2*$^{Cre/+}$; *Fgfr2*^{cnull} (*n=5,* independent biological replicates). Conversely, various chimerism in each cell type in *Foxa2*$^{Cre/+}$; *Fgfr2*^{hetero}; *Rosa*$^{tdTomato/+}$(*n=4*), *Shh*$^{Cre/+}$; *Fgfr2*^{cnull}; *Rosa*$^{tdTomato/+}$ (*n=2*), *Shh*$^{Cre/+}$; *Fgfr2*^{hetero}; *Rosa*$^{tdTomato/+}$(*n=3*), and *WT* (*n=7*). (E and F) Representative IF staining of E14.5 lung of *Fgfr2*^{cnull}. GFP and tdTomato indicate donor and host-derived cells, respectively. (E-F) Residual tdTomato^{+} host cells in E14.5 *Foxa2*$^{Cre/+}$; *Fgfr2*^{cnull} chimeric lungs. (F) Split images of (E) visualizing GFP^{+} donor cells and tdTomato^{+} host cells, co-stained with Ki67. (G) Graphs: % Ki67 labeling in mesenchymal cells of E14.5 *Foxa2*$^{Cre/+}$; *Fgfr2*^{cnull} chimeric lungs. Statistical analyses: paired Student's t-test, significance at $*P < 0.05$, ns: non-significant. Scale bars: B, C (left, right), E, F =1mm, 500μm, 50μm, 20μm, 20μm.

Methods

Mouse. *Shh*$^{Cre/+}$ mice (cat. 05622), *Rosa26*$^{tdTomato/\,tdTomato}$ mice (cat. 07914), Rosa26$^{nT\text{-}nG/nT\text{-}nG}$ mice (cat. 023035) and *Pdgfrα*$^{CreERT2/+}$ mice (cat. 032770) were obtained from the Jackson Lab. X. Zhang kindly gifted *Fgfr2*$^{flox/flox}$ mice. We further backcrossed these mice for over three generations with CD-1 mice (cat. 022) from the Charles River. Dr. Nicole C Dubois kindly provided *Foxa2*$^{Cre/Cre}$ mice. For conditional deletion of *Fgfr2* (*Fgfr2*^{cnull}), we crossed *Fgfr2*$^{flox/flox}$; *Rosa26*$^{tdTomato/tdTomato}$ females with *Foxa2*$^{Cre/Cre}$; *Fgfr2*$^{flox/+}$, *Foxa2*$^{Cre/+}$; *Fgfr2*$^{flox/+}$ or *Shh*$^{Cre/+}$; *Fgfr2*$^{flox/+}$ males, respectively. PCR performed genotyping of the *Shh-Cre*, *Pdgfr α-CreERT2*, *Rosa26-nTnG,* and *Rosa26-tdTomato* alleles according to the protocol provided by the vendor. For the CBC, genotyping of chimeric animals was confirmed by GFP-negative sorted liver cells and lung cells. For detecting the *Fgfr2* floxed allele, we performed PCR using the primer sets: FR2-F1, 5′-ATAGGAGCAACAGGCGG-3′, and FR2-F2, 5′-CAAGAGGCGACCAGTCA-3′[19]. For lineage tracing with Pdgfrα$^{CreERT2/+}$; Rosa26$^{tdTomato/+}$ mice, 1 dose of 200 µg tamoxifen (MedChem Express, HY-13757A) per g of body weight was given via oral gavage injection. All animal experiments were approved by Columbia University Institutional Animal Care and Use Committee in accordance with US National Institutes of Health guidelines.

Culture of mouse iPSC. We cultured iPSC in a2i/VPA/LIF medium on a feeder, as previously reported[19]. These PSC cells were passaged at a split ratio of 1:10 every 2–3 d.

Culture of human iPSCs (hiPSCs). All iPSC lines were maintained in feeder-free conditions on laminin iMatrix-511 silk E8 (Amsbio, AMS.892021) in StemFit 04 complete Medium (Amsbio, SFB-504), supplemented with Primocin (Invivogen, ant-pm-1), and passaged with TrypLE Select (Gibco, A1285901). All human iPSC lines used were characterized for pluripotency and were found to be karyotypically normal. The BU3NGST cell line was kindly gifted by Dr. Finn Hawkins and Dr. Darrell Kotton at Boston University, Boston, MA. Dr. Jennifer Davis, the University of Washington School of Medicine, Seattle, WA, kindly gifted the Rainbow cell line. PD2 and TD1 hiPSC were generated from deidentified commercially available human peripheral blood mononuclear cell and tracheal epithelial cell lines via the manufacturing protocol of Sendai virus-mediated reprogramming (CytoTune2.0) (ThermoFisher, A16517). Every other month, all iPSC lines screened negative for mycoplasma contamination using a MycoAlert PLUS detection kit (Lonza, LT07-710).

Differentiation of hiPSCs into lung epithelial and mesenchymal cells. The directed differentiation protocols were modified from previous protocols to maximize lung mesenchymal cell generation concomitantly with NKX2-1^{+} lung epithelium. Briefly, DE and LPM precursors were induced once seeded hiPSC-formed colonies by the Activin induction using the STEMdiff Definitive Endoderm Kit (StemCell Technologies, 05110) for 72 hours. Differentiated cells were dissociated and passaged in Laminin511-coated tissue culture plates in a complete serum-free differentiation medium (cSFDM)[35]. To induce DE and LPM into the anterior foregut endoderm and mesoderm, the cSFDM was supplemented with 10µM SB431542 (MedChem Express, HY-10431) and 2µM Dorsomorphin (Tocris, 3093) for 48 hours and 10µM SB431542 and 2µM IWP2 (Tocris, 3533) for 24 hours. Cells were then cultured for 7-10 additional days in cSFDM containing 3µM CHIR99021, 10ng/ml recombinant human FGF10 (R&D Systems, 345-FG), 10ng/ml recombinant human KGF (R&D Systems, 251-KG), 10 ng/mL recombinant human BMP4 (R&D

Systems, 314-BP), and 50nM retinoid acid (Sigma-Aldrich, R2625) to induce NKX2-1 positive lung epithelial cells and $WNT2^{+}TBX4^{+}$ lung mesenchymal cells.

Immunofluorescence (IF). Before the immunostaining, antigen retrieval was performed using Unmasking Solution (Vector Laboratories, H-3300) for 10 min at around 100 °C by microwave. 7-µm tissue sections were incubated with primary antibodies (Supplementary Table 1) in the buffer of M.O.M. kit (Vector Laboratories, MKB-2213-1) overnight at 4 °C, washed in PBS, and incubated with secondary antibodies conjugated with Alexa488, 567, or 647 (ThermoScientific, 1:400) with NucBlue Fixed Cell Ready Probes Reagent (Hoechst) (ThermoScientific, R37605) for 1.5 h, and mounted with ProLong Gold antifade reagent (Invitrogen, P36930). The images were captured by a Zeiss confocal 710 microscopy.

Immunocytochemistry. Cells on culture dishes were fixed with 4% Paraformaldehyde (PFA) for 30 min at room temperature (RT), permeabilized, and blocked with staining buffer containing 0.025% Triton X-100 and 1% BSA for 1 hour at RT. Primary antibodies (Supplementary Table 1) were incubated overnight at 4 °C in the staining buffer. After three washes in PBS, secondary antibodies (Supplementary Table 1) and NucBlue Fixed Cell Ready Probes Reagent (Hoechst) were incubated for 1 h. The samples were imaged using DMi8 Leica widefield microscope.

Flow cytometry (FCM) analyses of mouse lung tissue. Lungs from lineage tracing mice at E14.5, E18.5, P0, and four weeks were harvested and prepared for the FCM, as previously described[19]. Briefly, tissues were minced with microscissors, and 1 ml of pre-warmed dissociation buffer (1 mg/ml DNase (Sigma, DN25), 5 mg/ml collagen (Roche, 10103578001), and 15 U/ml Dispase II (Stemcell Technologies, 7913) in HBSS), incubated at 37 °C on the rocker with 50 r.p.m. speed, and neutralized with the dissociation buffer by FACS buffer containing 2% FBS, Glutamax, 2mM EDTA and 10mM HEPES in HBSS after the 30 min incubation. Digested cells were filtered by the. After filtrating the cells with a 40-µm filter (FALCON, 352235), cell pellets were resuspended with 1 ml of cold RBC lysis buffer (Biolegend, 420301) to lyse the remaining erythrocytes for 5 min on ice, and neutralized by 1 ml cold FACS buffer. After that, it was centrifuged them at 350 rcf, 4 °C, for 3 min to remove the lysed blood cells. For FCM analysis, one million cells were transferred in 100 µl of FACS buffer supplemented with 0.5µM Y27632 and then added 2 µl Fc Block (BD Pharmingen, 553141) per sample followed by 10 min incubation on ice. Cells were incubated with the following antibodies: CD31-APC (Biolegend, 102510, 1/50), Epcam-BV711 (BioLegend, 118233, 1/50), or Epcam-BV421 (Biolegend, 118225, 1/50), Aqua Zombie (BioLegend, 423101, 1/100), CD45-BV605 (BioLegend, 103104, 1/50) for 30 min on ice. After staining, cells were washed twice with FACS buffer before resuspending in 500 µl FACS buffer for the subsequent analyses using SONY MA900 or NovoCyte.

$nGFP^{+}$iPSC establishment and preparation for CBC donor.
E14.5 lung tissues of *Rosa26*$^{nTnG/nTnG}$ mice (JAX, cat. 023035, C57BL/6NJ background) were harvested in a dissociation buffer described above. The dissociated cells were seeded on a 10cm dish, and only lung fibroblast survived after 1 week in MEF medium[19]. The fibroblasts were passaged using Accutase (Innovative Cell Technologies, AT104) and seeded on gelatin (Millipore-Sigma, ES006B)-coated 6-well plates with a density of 0.1 million cells per well. Upon cell attachment, Yamanaka reprogramming factors were induced to iPSCs via Sendai virus using CytoTune2.0 (ThermoFisher, A16517). To establish $nGFP^{+}$ iPSCs, the Cre plasmid was

transfected using Fugene HD transfection reagent (Promega, E2311), then sorted out $GFP^{+}tdTomato^{-}$ live cells by FACS (SONYMA900), and single clones were expanded.

For the CBC donor cell preparation, $nGFP^{+}$iPSCs cultured in a2i/VPA/LIF[19] were trypsinized and resuspended in 4 ml cold DMEM + 10% FBS immediately and filtering the cells with a 40-μm filter. Cells were centrifuged at 350 rcf, 4 °C, for 3 min, and the supernatant was removed. After being washed with flow buffer containing 0.2% BSA, 1% Glutamax, and 1μM Y27632, the cells were resuspended in 100μl/1 million cells with flow buffer. The following antibodies were added: Epcam-BV421 (1:50), SSEA1-PE (1:50), CD31-APC (1:50), Zombie Aqua Fixable Viability Kit (1:100). $Epcam^{high}SSEA1^{high}CD31^{high}$ cells were sorted by FACS (SONYMA900) and subsequently prepared for the injection.

Blastocyst preparation and embryo transfer. Blastocysts were prepared by mating $Foxa2^{Cre/Cre}$; $Fgfr2^{flox/+}$, $Foxa2^{Cre/+}$; $Fgfr2^{flox/+}$ or $Shh^{Cre/+}$; $Fgfr2^{flox/+}$ males (all 129 x B6 x CD-1 background) with superovulated $Fgfr2^{flox/flox}$; $Rosa26^{tdTomato/tdTomato}$ females (129 x B6 x CD-1 background). Blastocysts were harvested at E3.5 after superovulation[19]. 20 sorted $nGFP^{+}$iPSCs were injected into each blastocyst. After the iPSC injection, blastocysts were cultured in an M2 medium (Cosmobio) for a few hours in a 37 °C, 5% CO2 incubator for recovery. Then, blastocysts were transferred to the uterus of the pseudopregnant foster mother.

Real-time-quantitative RT-PCR (qRT-PCR). Total RNA was extracted using a Direct-zol™ RNA MiniPrep Plus kit (Zymo Research, R2072), and cDNA was synthesized using Primescript™ RT Master Mix (Takara, RR036B). The cDNAs were then used as templates for qRT-PCR analysis with gene-specific primers. Reactions (10 μl) were performed Luna® Universal qPCR Master Mix (New England Biolabs, M3003X). mRNA abundance for each gene was determined relative to GAPDH mRNA using the $2^{-\Delta\Delta Ct}$ method. The primers were listed in the Supplemental Table. 2. Data were represented as mean ± SD of measurements. The number of animals or cells per group is provided in the legends. The undetected values in each biological experiment in Fig.3d were removed from the graphs.

Statistical analysis. Data analysis was performed using Prism 8. Data acquired by performing biological replicas of two or three independent experiments are presented as the mean ± SD. Statistical significance was determined using a two-tailed t-test and unpaired one-way or two-way ANOVA with the Tukey post hoc test. $*P < 0.05$, $**P < 0.01$, $***P < 0.001$, ns: non-significant.

Data availability. The authors declare that all data supporting the results of this study are available within the paper and the Supplementary Information. Raw data are available from the corresponding author upon reasonable request.

References

1. Wang, X. (2019). Bioartificial Organ Manufacturing Technologies. Cell Transplant *28*, 5–17. 10.1177/0963689718809918.
2. Ott, H.C., Clippinger, B., Conrad, C., Schuetz, C., Pomerantseva, I., Ikonomou, L., Kotton, D., and Vacanti, J.P. (2010). Regeneration and orthotopic transplantation of a bioartificial lung. Nat Med *16*, 927–933. 10.1038/nm.2193.

3. Petersen, T.H., Calle, E.A., Zhao, L., Lee, E.J., Gui, L., Raredon, M.S.B., Gavrilov, K., Yi, T., Zhuang, Z.W., Breuer, C., et al. (2010). Tissue-engineered lungs for in vivo implantation. Science (1979) *329*, 538–541. 10.1126/science.1189345.
4. Hackett, T.L., Knight, D. a, and Sin, D.D. (2010). Potential role of stem cells in management of COPD. Int J Chron Obstruct Pulmon Dis *5*, 81–88.
5. Kemter, E., Schnieke, A., Fischer, K., Cowan, P.J., and Wolf, E. (2020). Xeno-organ donor pigs with multiple genetic modifications - the more the better? Curr Opin Genet Dev *64*, 60–65. 10.1016/J.GDE.2020.05.034.
6. Kotton, D.N., and Morrisey, E.E. (2014). Lung regeneration: Mechanisms, applications and emerging stem cell populations. Nat Med *20*, 822–832. 10.1038/nm.3642.
7. Tian, L., Gao, J., Garcia, I.M., Chen, H.J., Castaldi, A., and Chen, Y.W. (2021). Human pluripotent stem cell-derived lung organoids: Potential applications in development and disease modeling. Wiley Interdiscip Rev Dev Biol *10*, 1–16. 10.1002/wdev.399.
8. Guyette, J.P., Gilpin, S.E., Charest, J.M., Tapias, L.F., Ren, X., and Ott, H.C. (2014). Perfusion decellularization of whole organs. Nat Protoc *9*, 1451–1468. 10.1038/nprot.2014.097.
9. Travaglini, K.J., Nabhan, A.N., Penland, L., Sinha, R., Gillich, A., Sit, R. v., Chang, S., Conley, S.D., Mori, Y., Seita, J., et al. (2020). A molecular cell atlas of the human lung from single-cell RNA sequencing. Nature *587*, 619–625. 10.1038/s41586-020-2922-4.
10. Crapo, J.D., Barry, B.E., Gehr, P., Bachofen, M., and Weibel, E.R. (1982). Cell number and cell characteristics of the normal human lung. American Review of Respiratory Disease *126*, 332–337. 10.1164/arrd.1982.126.2.332.
11. Stone, K.C., Mercer, R.R., Gehr, P., Stockstill, B., and Crapo, J.D. (1992). Allometric Relationships of Cell Numbers and Size in the Mammalian Lung. Am. J. Respir. Cell Mol. BioI. *6*, 235–243.
12. Chen, J., Lansford, R., Stewart, V., Young, F., and Alt, F.W. (1993). RAG-2-deficient blastocyst complementation: an assay of gene function in lymphocyte development. Proceedings of the National Academy of Sciences *90*, 4528–4532. 10.1073/pnas.90.10.4528.
13. Usui, J., Kobayashi, T., Yamaguchi, T., Knisely, a S., Nishinakamura, R., and Nakauchi, H. (2012). Generation of kidney from pluripotent stem cells via blastocyst complementation. Am J Pathol *180*, 2417–2426. 10.1016/j.ajpath.2012.03.007.
14. Yamaguchi, T., Sato, H., Kato-Itoh, M., Goto, T., Hara, H., Sanbo, M., Mizuno, N., Kobayashi, T., Yanagida, A., Umino, A., et al. (2017). Interspecies organogenesis generates autologous functional islets. Nature *542*, 191–196. 10.1038/nature21070.
15. Hamanaka, S., Umino, A., Sato, H., Hayama, T., Yanagida, A., Mizuno, N., Kobayashi, T., Kasai, M., Suchy, F.P., Yamazaki, S., et al. (2018). Generation of Vascular Endothelial Cells and Hematopoietic Cells by Blastocyst Complementation. Stem Cell Reports *11*, 988–997. 10.1016/j.stemcr.2018.08.015.
16. Kobayashi, T., Yamaguchi, T., Hamanaka, S., Kato-Itoh, M., Yamazaki, Y., Ibata, M., Sato, H., Lee, Y.-S., Usui, J.-I., Knisely, a S., et al. (2010). Generation of rat pancreas in mouse by interspecific blastocyst injection of pluripotent stem cells. Cell *142*, 787–799. 10.1016/j.cell.2010.07.039.
17. Kitahara, A., Ran, Q., Oda, K., Yasue, A., Abe, M., Ye, X., Sasaoka, T., Tsuchida, M., Sakimura, K., Ajioka, Y., et al. (2020). Generation of Lungs by Blastocyst

Complementation in Apneumic Fgf10-Deficient Mice. Cell Rep *31*, 107626. 10.1016/J.CELREP.2020.107626.

18. Li, E., Ustiyan, V., Wen, B., Kalin, G.T., Whitsett, J.A., Kalin, T. v., and Kalinichenko, V. v. (2021). Blastocyst complementation reveals that NKX2-1 establishes the proximal-peripheral boundary of the airway epithelium. Dev Dyn *250*, 1001–1020. 10.1002/DVDY.298.
19. Mori, M., Furuhashi, K., Danielsson, J.A., Hirata, Y., Kakiuchi, M., Lin, C.S., Ohta, M., Riccio, P., Takahashi, Y., Xu, X., et al. (2019). Generation of functional lungs via conditional blastocyst complementation using pluripotent stem cells. Nat Med *25*, 1691–1698. 10.1038/s41591-019-0635-8.
20. Kitahara, A., Ran, Q., Oda, K., Yasue, A., Abe, M., Ye, X., Sasaoka, T., Tsuchida, M., Sakimura, K., Ajioka, Y., et al. (2020). Generation of Lungs by Blastocyst Complementation in Apneumic Fgf10-Deficient Mice. Cell Rep *31*. 10.1016/j.celrep.2020.107626.
21. Wen, B., Li, E., Ustiyan, V., Wang, G., Guo, M., Na, C.L., Kalin, G.T., Galvan, V., Xu, Y., Weaver, T.E., et al. (2021). In vivo generation of lung and thyroid tissues from embryonic stem cells using blastocyst complementation. Am J Respir Crit Care Med *203*, 471–483. 10.1164/rccm.201909-1836OC.
22. Green, M.D., Chen, A., Nostro, M.-C., d'Souza, S.L., Schaniel, C., Lemischka, I.R., Gouon-Evans, V., Keller, G., and Snoeck, H.-W. (2011). Generation of anterior foregut endoderm from human embryonic and induced pluripotent stem cells. Nat Biotechnol *29*, 267–272. 10.1038/nbt.1788.
23. Huang, S.X.L., Islam, M.N., O'Neill, J., Hu, Z., Yang, Y.-G., Chen, Y.-W., Mumau, M., Green, M.D., Vunjak-Novakovic, G., Bhattacharya, J., et al. (2014). Efficient generation of lung and airway epithelial cells from human pluripotent stem cells. Nat Biotechnol *32*, 84–91. 10.1038/nbt.2754.
24. Han, L., Chaturvedi, P., Kishimoto, K., Koike, H., Nasr, T., Iwasawa, K., Giesbrecht, K., Witcher, P.C., Eicher, A., Haines, L., et al. (2020). Single cell transcriptomics identifies a signaling network coordinating endoderm and mesoderm diversification during foregut organogenesis. Nat Commun *11*. 10.1038/s41467-020-17968-x.
25. Tada, S., Era, T., Furusawa, C., Sakurai, H., Nishikawa, S., Kinoshita, M., Nakao, K., Chiba, T., and Nishikawa, S.I. (2005). Characterization of mesendoderm: A diverging point of the definitive endoderm and mesoderm in embryonic stem cell differentiation culture. Development *132*, 4363–4374. 10.1242/dev.02005.
26. Hart, A.H., Hartley, L., Sourris, K., Stadler, E.S., Li, R., Stanley, E.G., Tam, P.P.L., Elefanty, A.G., and Robb, L. (2002). Mixl1 is required for axial mesendoderm morphogenesis and patterning in the murine embryo. Development *129*, 3597–3608.
27. Wan, H., Kaestner, K.H., Ang, S.L., Ikegami, M., Finkelman, F.D., Stahlman, M.T., Fulkerson, P.C., Rothenberg, M.E., and Whitsett, J.A. (2004). Foxa2 regulates alveolarization and goblet cell hyperplasia. Development *131*, 953–964. 10.1242/dev.00966.
28. Scheibner, K., Schirge, S., Burtscher, I., Büttner, M., Sterr, M., Yang, D., Böttcher, A., Ansarullah, Irmler, M., Beckers, J., et al. (2021). Epithelial cell plasticity drives endoderm formation during gastrulation. Nat Cell Biol *23*, 692–703. 10.1038/s41556-021-00694-x.

29. Kopper, O., and Benvenisty, N. (2012). Stepwise differentiation of human embryonic stem cells into early endoderm derivatives and their molecular characterization. Stem Cell Res *8*, 335–345. 10.1016/j.scr.2011.12.006.
30. Artus, J., Panthier, J.J., and Hadjantonakis, A.K. (2010). A role for PDGF signaling in expansion of the extra-embryonic endoderm lineage of the mouse blastocyst. Development *137*, 3361–3372. 10.1242/dev.050864.
31. Horn, S., Kobberup, S., Jørgensen, M.C., Kalisz, M., Klein, T., Kageyama, R., Gegg, M., Lickert, H., Lindner, J., Magnuson, M.A., et al. (2012). Mind bomb 1 is required for pancreatic β-cell formation. Proc Natl Acad Sci U S A *109*, 7356–7361. 10.1073/pnas.1203605109.
32. Peng, T., Tian, Y., Boogerd, C.J., Lu, M.M., Kadzik, R.S., Stewart, K.M., Evans, S.M., and Morrisey, E.E. (2013). Coordination of heart and lung co-development by a multipotent cardiopulmonary progenitor. Nature *500*, 589–592. 10.1038/nature12358.
33. Bardot, E., Calderon, D., Santoriello, F., Han, S., Cheung, K., Jadhav, B., Burtscher, I., Artap, S., Jain, R., Epstein, J., et al. (2017). Foxa2 identifies a cardiac progenitor population with ventricular differentiation potential. Nat Commun *8*, 1–15. 10.1038/ncomms14428.
34. Hawkins, F., Kramer, P., Jacob, A., Driver, I., Thomas, D.C., Mccauley, K.B., Skvir, N., Crane, A.M., Kurmann, A.A., Hollenberg, A.N., et al. (2017). Prospective isolation of NKX2-1 – expressing human lung progenitors derived from pluripotent stem cells. J Clin Invest *127*, 1–18. 10.1172/JCI89950.
35. Chen, Y.-W., Huang, S.X., de Carvalho, A.L.R.T., Ho, S.-H., Islam, M.N., Volpi, S., Notarangelo, L.D., Ciancanelli, M., Casanova, J.-L., Bhattacharya, J., et al. (2017). A three-dimensional model of human lung development and disease from pluripotent stem cells. Nat Cell Biol *19*, 542–549. 10.1038/ncb3510.
36. Gotoh, S., Ito, I., Nagasaki, T., Yamamoto, Y., Konishi, S., Korogi, Y., Matsumoto, H., Muro, S., Hirai, T., Funato, M., et al. (2014). Generation of alveolar epithelial spheroids via isolated progenitor cells from human pluripotent stem cells. Stem Cell Reports *3*, 394–403. 10.1016/j.stemcr.2014.07.005.
37. Konishi, S., Gotoh, S., Tateishi, K., Yamamoto, Y., Korogi, Y., Nagasaki, T., Matsumoto, H., Muro, S., Hirai, T., Ito, I., et al. (2016). Directed Induction of Functional Multi-ciliated Cells in Proximal Airway Epithelial Spheroids from Human Pluripotent Stem Cells. Stem Cell Reports *6*, 18–25. 10.1016/j.stemcr.2015.11.010.
38. De Langhe, S.P., Carraro, G., Warburton, D., Hajihosseini, M.K., and Bellusci, S. (2006). Levels of mesenchymal FGFR2 signaling modulate smooth muscle progenitor cell commitment in the lung. Dev Biol *299*, 52–62. 10.1016/j.ydbio.2006.07.001.
39. De Moerlooze, L., Spencer-Dene, B., Revest, J.M., Hajihosseini, M., Rosewell, I., and Dickson, C. (2000). An important role for the IIIb isoform of fibroblast growth factor receptor 2 (FGFR2) in mesenchymal-epithelial signalling during mouse organogenesis. Development *127*, 483–492.
40. Arman, E., Haffner-Krausz, R., Gorivodsky, M., and Lonai, P. (1999). Fgfr2 is required for limb outgrowth and lung-branching morphogenesis. Proceedings of the National Academy of Sciences *96*, 11895–11899. 10.1073/pnas.96.21.11895.
41. Sekine, K., Ohuchi, H., Fujiwara, M., Yamasaki, M., Yoshizawa, T., Sato, T., Yagishita, N., Matsui, D., Koga, Y., Itoh, N., et al. (1999). Fgf10 is essential for limb and lung formation. Nat Genet *21*, 138–141. 10.1038/5096.

42. Mori, M., Furuhashi, K., Danielsson, J.A., Hirata, Y., Kakiuchi, M., Lin, C.S., Ohta, M., Riccio, P., Takahashi, Y., Xu, X., et al. (2019). Generation of functional lungs via conditional blastocyst complementation using pluripotent stem cells. Nature Medicine 2019 25:11 *25*, 1691–1698. 10.1038/s41591-019-0635-8.
43. Pijuan-Sala, B., Griffiths, J.A., Guibentif, C., Hiscock, T.W., Jawaid, W., Calero-Nieto, F.J., Mulas, C., Ibarra-Soria, X., Tyser, R.C.V., Ho, D.L.L., et al. (2019). A single-cell molecular map of mouse gastrulation and early organogenesis. Nature *566*, 490–495. 10.1038/s41586-019-0933-9.